6-24-2009

π^+ Photoproduction on the Proton for Photon Energies from 0.725 to 2.875 GeV

M. Dugger

Gerard P. Gilfoyle
University of Richmond, ggilfoyl@richmond.edu

et. al.

Recommended Citation

Dugger, M., B. Ritchie, J. Ball, P. Collins, E. Pasyuk, R. Arndt, W. Briscoe, I. Strakovsky, R. Workman, M. Amaryan, M. Anghinolfi, H. Bagdasaryan, M. Battaglieri, M. Bellis, B. Berman, A. Biselli, C. Bookwalter, D. Branford, W. Brooks, V. Burkert, S. Careccia, D. Carman, P. Cole, P. Corvisiero, V. Crede, A. Daniel, N. Dashyan, R. Vita, E. Sanctis, A. Deur, S. Dhamija, R. Dickson, C. Djalali, G. Dodge, D. Doughty, P. Eugenio, G. Fedotov, J. Ficenec, A. Fradi, G. Gilfoyle, K. Giovanetti, F. Girod, W. Gohn, R. Gothe, K. Griffioen, M. Guidal, K. Hafidi, H. Hakobyan, C. Hanretty, N. Hassall, D. Heddle, K. Hicks, M. Holtrop, C. Hyde, Y. Ilieva, D. Ireland, B. Ishkhanov, E. Isupov, J. Johnstone, K. Joo, D. Keller, M. Khandaker, P. Khetarpal, W. Kim, A. Klein, F. Klein, L. Kramer, V. Kubarovsky, S. Kuleshov, V. Kuznetsov, K. Livingston, H. Lu, M. McCracken, B. McKinnon, C. Meyer, M. Mirazita, V. Mokeev, B. Moreno, K. Moriya, P. Nadel-Turonski, R. Nasseripour, S. Niccolai, I. Niculescu, M. Niroula, M. Osipenko, A. Ostrovidov, S. Park, S. Pereira, O. Pogorelko, S. Pozdniakov, J. Price, S. Procureur, D. Protopopescu, B. Raue, G. Ricco, M. Ripani, G. Rosner, P. Rossi, F. Sabatié, M. Saini, J. Salamanca, C. Salgado, R. Schumacher, Y. Sharabian, D. Sober, D. Sokhan, S. Stepanyan, S. Stepanyan, S. Strauch, M. Taiuti, D. Tedeschi, S. Tkachenko, M. Vineyard, D. Watts, L. Weinstein, D. Weygand, M. Wood, and A. Yegneswaran. "π+ Photoproduction on the Proton for Photon Energies from 0.725 to 2.875 GeV." *Physical Review C* 79, no. 6 (2009): 065206: 1-14. doi:10.1103/PhysRevC.79.065206.

π^+ photoproduction on the proton for photon energies from 0.725 to 2.875 GeV

M. Dugger,[2] B. G. Ritchie,[2] J. P. Ball,[2] P. Collins,[2] E. Pasyuk,[2] R. A. Arndt,[13] W. J. Briscoe,[13] I. I. Strakovsky,[13] R. L. Workman,[13] M. J. Amaryan,[25] M. Anghinolfi,[17] H. Bagdasaryan,[25,*] M. Battaglieri,[17] M. Bellis,[4] B. L. Berman,[13] A. S. Biselli,[10,26] C. Bookwalter,[12] D. Branford,[9] W. K. Brooks,[30,32] V. D. Burkert,[30] S. L. Careccia,[25] D. S. Carman,[30] P. L. Cole,[15,30] P. Corvisiero,[17] V. Crede,[12] A. Daniel,[24] N. Dashyan,[36] R. De Vita,[17] E. De Sanctis,[16] A. Deur,[30] S. Dhamija,[11] R. Dickson,[4] C. Djalali,[29] G. E. Dodge,[25] D. Doughty,[7,30] P. Eugenio,[12] G. Fedotov,[28] J. Ficenec,[33] A. Fradi,[18,33] G. P. Gilfoyle,[27] K. L. Giovanetti,[20] F. X. Girod,[6,†] W. Gohn,[8] R. W. Gothe,[29] K. A. Griffioen,[35] M. Guidal,[18] K. Hafidi,[1] H. Hakobyan,[36] C. Hanretty,[12] N. Hassall,[14] D. Heddle,[7,30] K. Hicks,[24] M. Holtrop,[22] C. E. Hyde,[25] Y. Ilieva,[29] D. G. Ireland,[14] B. S. Ishkhanov,[28] E. L. Isupov,[28] J. R. Johnstone,[14] K. Joo,[8,34] D. Keller,[24] M. Khandaker,[23] P. Khetarpal,[26] W. Kim,[21] A. Klein,[25] F. J. Klein,[5,30] L. H. Kramer,[11,30] V. Kubarovsky,[30] S. V. Kuleshov,[19,‡] V. Kuznetsov,[21] K. Livingston,[14] H. Y. Lu,[29] M. E. McCracken,[4] B. McKinnon,[14] C. A. Meyer,[4] M. Mirazita,[16] V. Mokeev,[28,30] B. Moreno,[18] K. Moriya,[4] P. Nadel-Turonski,[5] R. Nasseripour,[29,§] S. Niccolai,[18] I. Niculescu,[13,20] M. R. Niroula,[25] M. Osipenko,[17,28] A. I. Ostrovidov,[12] S. Park,[12] S. Anefalos Pereira,[16] O. Pogorelko,[19] S. Pozdniakov,[19] J. W. Price,[3] S. Procureur,[6] D. Protopopescu,[14] B. A. Raue,[11,30] G. Ricco,[17] M. Ripani,[17] G. Rosner,[14] P. Rossi,[16] F. Sabatié,[6,25] M. S. Saini,[12] J. Salamanca,[15] C. Salgado,[23] R. A. Schumacher,[4] Y. G. Sharabian,[30,36] D. I. Sober,[5] D. Sokhan,[9] S. Stepanyan,[30,36] S. S. Stepanyan,[21] S. Strauch,[29] M. Taiuti,[17] D. J. Tedeschi,[29] S. Tkachenko,[25] M. F. Vineyard,[27,31] D. P. Watts,[14,‖] L. B. Weinstein,[25] D. P. Weygand,[30] M. H. Wood,[29] and A. Yegneswaran[30]

(CLAS Collaboration)

[1]*Argonne National Laboratory, Argonne, IL 60439, USA*
[2]*Arizona State University, Tempe, Arizona 85287-1504, USA*
[3]*California State University, Dominguez Hills, Carson, California 90747, USA*
[4]*Carnegie Mellon University, Pittsburgh, Pennsylvania 15213, USA*
[5]*Catholic University of America, Washington, DC 20064, USA*
[6]*CEA-Saclay, Service de Physique Nucléaire, F-91191 Gif-sur-Yvette, France*
[7]*Christopher Newport University, Newport News, Virginia 23606, USA*
[8]*University of Connecticut, Storrs, Connecticut 06269, USA*
[9]*Edinburgh University, Edinburgh EH9 3JZ, United Kingdom*
[10]*Fairfield University, Fairfield, Connecticut 06824, USA*
[11]*Florida International University, Miami, Florida 33199, USA*
[12]*Florida State University, Tallahassee, Florida 32306, USA*
[13]*The George Washington University, Washington, DC 20052, USA*
[14]*University of Glasgow, Glasgow G12 8QQ, United Kingdom*
[15]*Idaho State University, Pocatello, Idaho 83209, USA*
[16]*INFN, Laboratori Nazionali di Frascati, I-00044 Frascati, Italy*
[17]*INFN, Sezione di Genova, I-16146 Genova, Italy*
[18]*Institut de Physique Nucleaire ORSAY, Orsay, France*
[19]*Institute of Theoretical and Experimental Physics, Moscow RU-117259, Russia*
[20]*James Madison University, Harrisonburg, Virginia 22807, USA*
[21]*Kyungpook National University, Daegu 702-701, Republic of Korea*
[22]*University of New Hampshire, Durham, New Hampshire 03824-3568, USA*
[23]*Norfolk State University, Norfolk, Virginia 23504, USA*
[24]*Ohio University, Athens, Ohio 45701, USA*
[25]*Old Dominion University, Norfolk, Virginia 23529, USA*
[26]*Rensselaer Polytechnic Institute, Troy, New York 12180-3590, USA*
[27]*University of Richmond, Richmond, Virginia 23173, USA*
[28]*Skobeltsyn Nuclear Physics Institute, Moscow RU-119899, Russia*
[29]*University of South Carolina, Columbia, South Carolina 29208, USA*
[30]*Thomas Jefferson National Accelerator Facility, Newport News, Virginia 23606, USA*
[31]*Union College, Schenectady, New York 12308, USA*
[32]*Universidad Técnica Federico Santa María, Casilla 110-V Valparaíso, Chile*
[33]*Virginia Polytechnic Institute and State University, Blacksburg, Virginia 24061-0435, USA*
[34]*University of Virginia, Charlottesville, Virginia 22901, USA*
[35]*College of William and Mary, Williamsburg, Virginia 23187-8795, USA*
[36]*Yerevan Physics Institute, 375036 Yerevan, Armenia*

(Received 6 March 2009; published 24 June 2009)

Differential cross sections for the reaction $\gamma p \to n\pi^+$ have been measured with the CEBAF Large Acceptance Spectrometer (CLAS) and a tagged photon beam with energies from 0.725 to 2.875 GeV. Where available, the results obtained here compare well with previously published results for the reaction. Agreement with the SAID and MAID analyses is found below 1 GeV. The present set of cross sections has been incorporated into the SAID database, and exploratory fits have been made up to 2.7 GeV. Resonance couplings have been extracted and compared to previous determinations. With the addition of these cross sections to the world data set, significant changes have occurred in the high-energy behavior of the SAID cross-section predictions and amplitudes.

DOI: 10.1103/PhysRevC.79.065206 PACS number(s): 13.60.Le, 14.20.Gk, 13.30.Eg, 13.75.Gx

I. INTRODUCTION

The photoproduction of mesons has played a crucial role in the search for resonances beyond those found through analyses of pion-nucleon elastic scattering data. Cross section structures seen in kaon and eta photoproduction [1] have been interpreted as candidates for so-called missing resonances, excitations that are predicted by QCD-inspired models [2] but expected to couple weakly to the pion-nucleon channel.

The photoproduction of pions, though less likely to detect states not seen in pion-nucleon studies, is the most well-developed of the meson-photoproduction programs, having an extensive database for which many single- and multi-channel fits are available [3]. The photo-decay amplitudes for nonstrange resonances have been determined almost exclusively from this reaction [4]. However, although cross section data exist, they are quite sparse above an incident photon energy $E_\gamma = 1.7$ GeV and have generally come from untagged bremsstrahlung measurements. As a result, all photo-decay amplitudes for the higher N^* states have an inherent uncertainty beyond any model dependence owing to the background-resonance extraction process. Although some theory-based model dependence is unavoidable, cross sections measured precisely using a tagged-photon beam, with incident photon energies covering the full resonance region, will provide tighter and more reliable constraints for future analyses of the properties of excited nucleons.

In this paper, we report measurements of the unpolarized differential cross sections for π^+ photoproduction on the proton for E_γ from 0.725 to 2.875 GeV. As a first step to gauge their influence, we have included these new cross sections in a multipole fit to all available data covering the resonance region. This task is aided by the inclusion of tagged neutral pion cross sections recently measured [5] that span a range in E_γ from 0.675 to 2.875 GeV. We have obtained a revised set of multipole amplitudes and have extracted photo-decay couplings for those states that couple strongly to the pion-nucleon final state. Using the revised multipole analysis, we have generated predictions for further measurements of polarization observables that should soon become available.

The paper is laid out in the following manner: We give a brief background of the experimental parameters for this study in Sec. II. An overview of the method used is given in Sec. III. The uncertainty estimates for the cross sections obtained are given in Sec. IV. The experimental results are described in Sec. V. Various fits to the data are described in Sec. VI, and the underlying multipole amplitudes and resonance contributions are displayed and compared to previous determinations in Sec. VII. Finally, in Sec. VIII, we provide a brief summary of the results of the study and consider what extensions of this work would be particularly helpful in the future.

II. EXPERIMENT

The differential cross sections for the reaction $\gamma p \to n\pi^+$ were measured with the CEBAF Large Acceptance Spectrometer (CLAS) [6] and the bremsstrahlung photon-tagging facility ("photon tagger") [7] in Hall B of the Thomas Jefferson National Accelerator Facility (JLab) as part of a set of experiments running at the same time with the same experimental configuration (cryogenic target, tagger, and CLAS) called the "g1c" run period. The cross sections were part of a program of meson photoproduction measurements undertaken using CLAS and the photon tagger [5,8–15].

The data described here were obtained in sets of data runs with differing energies for the electron beam incident on the photon tagger. The two incident electron energies were 2.445 and 3.115 GeV. Moreover, the 3.115-GeV data runs were taken with either the full photon-tagger focal plane ("3.115-full") or higher photon-energy half of the photon-tagger focal plane ("3.115-half") in operation. Thus, for example, during the 3.115-half running, data were accumulated only for the higher energy half of the available photon energies to increase statistics for data collected at those higher energies.

The produced tagged photons impinged on an 18-cm-long liquid-hydrogen target placed at the center of CLAS. This target was enclosed by a scintillator array (called the "start counter," described in Ref. [16]) that detected the passage of charged particles into CLAS from the target. The event trigger required the coincidence of a post-bremsstrahlung electron passing through the focal plane of the photon tagger and at least one charged particle detected in CLAS and the start counter. Tracking of the charged particles through the magnetic field within CLAS by drift chambers [17] provided determination of their charge, momentum, and scattering

*Current address: University of Virginia, Charlottesville, Virginia 22901, USA.
†Current address: Thomas Jefferson National Accelerator Facility, Newport News, Virginia 23606, USA.
‡Current address: Universidad Técnica Federico Santa María, Casilla 110-V Valparaíso, Chile.
§Current address: The George Washington University, Washington, DC 20052, USA.
‖Current address: Edinburgh University, Edinburgh EH9 3JZ, United Kingdom.

angle. This information, together with the particle velocity measured by the time-of-flight system [18] and start counter, provided particle identification for each particle detected in CLAS and its corresponding momentum four-vector.

The methods used for extracting the differential cross sections for π^+ photoproduction are presented in the next several sections. The technique is outlined initially, and then each step is described in further detail, with a summary provided of the data and tests that support the validity of the approach taken.

III. DATA REDUCTION

The technique for this analysis is very similar to that used previously in the analysis of the CLAS g1c running period data for the reaction $\gamma p \to p\pi^0$ [5]. In that analysis, the recoiling proton from the photoproduction process was detected in CLAS and, by assuming the two-body reaction $\gamma p \to pX$ (where X was the undetected π^0), yields were determined in the missing mass spectra for the reconstructed π^0.

In this analysis, similarly, the photoproduced π^+ was detected in CLAS. Again assuming the two-body reaction $\gamma p \to \pi^+ X$, where in the present case X was the undetected neutron, we determined yields in the missing mass spectra for the reconstructed neutron. However, although both the proton and π^+ are positively charged particles, the CLAS detector response to the recoiling pions and protons was different (e.g., the amount of energy deposited in the scintillators within the detector), which necessitated appropriate modifications to the previous analysis.

For the data described in this paper, yields for the neutron were determined using the following steps:

(i) Identify the π^+ in CLAS, determining the scattering angle and momentum.
(ii) Sort the events in the resulting missing mass spectra into kinematic bins in incident photon energy E_γ and scattering angle $\theta^\pi_{\text{c.m.}}$, where $\theta^\pi_{\text{c.m.}}$ is the center-of-mass angle of the π^+.
(iii) Identify the missing mass peak for the neutron in each kinematic bin.
(iv) Determine the yield for the neutron in each kinematic bin by subtracting the background beneath the peak.
(v) Correct the meson yield in each kinematic bin for spectrometer acceptance using a Monte Carlo simulation of the spectrometer acceptance.
(vi) Normalize the measured yield in each kinematic bin using a measured absolute photon flux normalization procedure, thereby determining the differential cross section for that bin.

In the following sections, each of these steps is described. Also presented are sample results, and, in some cases, tests that establish the validity of the procedures used.

A. Particle identification and kinematic variables

The tracking information provided by the drift chambers within CLAS gave momentum and scattering angle information on charged particles scattered within the detector volume. Time-of-flight and start counter information, coupled with the track information provided by the drift chambers, determined particle velocity and momentum.

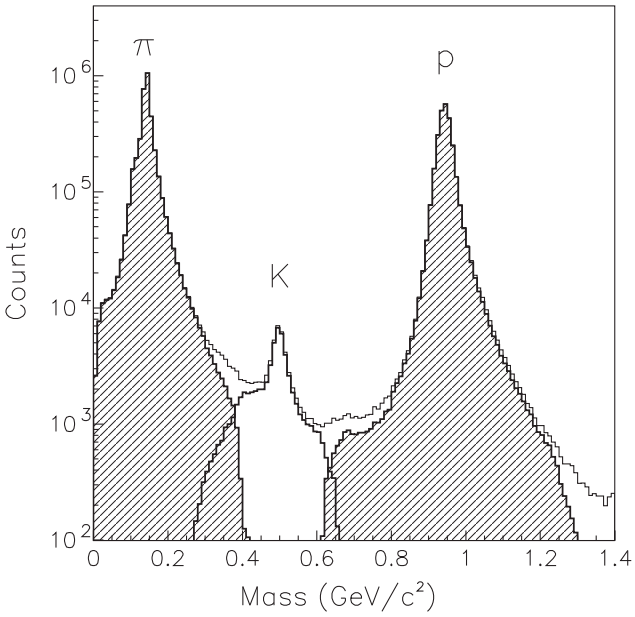

FIG. 1. Particle identification spectrum obtained with CLAS, showing identifications provided by the GPID algorithm (discussed in the text) for all charged particles.

Particle identification in this analysis was performed using the GPID algorithm [19]. The method uses the momentum of the detected particle, and sequentially calculates trial values of the velocity β for all possible particle identities. Each one of the possible identities is tested by comparing the trial value of β for a given particle type to the empirically measured value of β (as determined by CLAS tracking and time-of-flight information). The particle is assigned the identity that provides the closest trial value of β to the empirically measured value of β. For example, if the curvature indicates a positive particle, the β value is calculated for p, π^+, and K^+. Figure 1 shows the mass distribution of the identified charged particles. The GPID algorithm also attempts to find a matching photon in the tagging system for every charged particle detected in CLAS. A matched photon means that there was one and only one tagged photon in the trigger window, which, in this analysis, was 18 ns. Particles that were determined not to have a matching photon are considered to be a measure of the accidentals (to be described in more detail in the next section).

CLAS is divided into six sectors in azimuthal angle. Geometrical fiducial cuts in each of the six sectors of CLAS were imposed on all pions. The region selected for accepting pions in each sector corresponded to a region of relatively uniform detection efficiency (constant to $\pm 3\%$) versus azimuthal angle.

B. Missing mass reconstruction

The momentum for the π^+ was determined by the drift chamber system. The momentum determined by CLAS was corrected for energy loss in both the target cell and the start counter [20]. The scattering angle and momentum were used to calculate the missing mass based on the assumption that the reaction observed is $\pi^+ X$. Based on this assumption, the

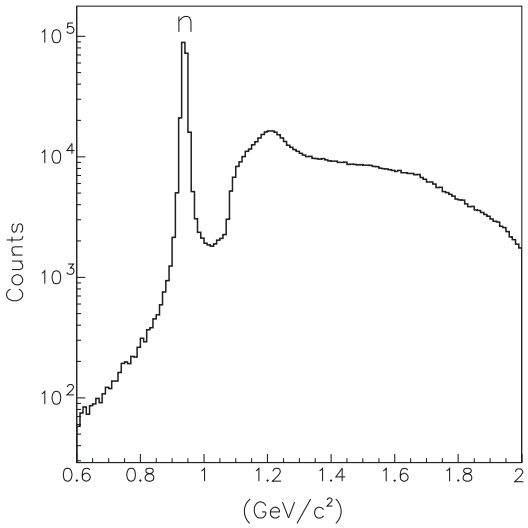

FIG. 2. Missing mass spectrum obtained from the g1c data set using CLAS and assuming the reaction $\gamma p \to \pi^+ X$.

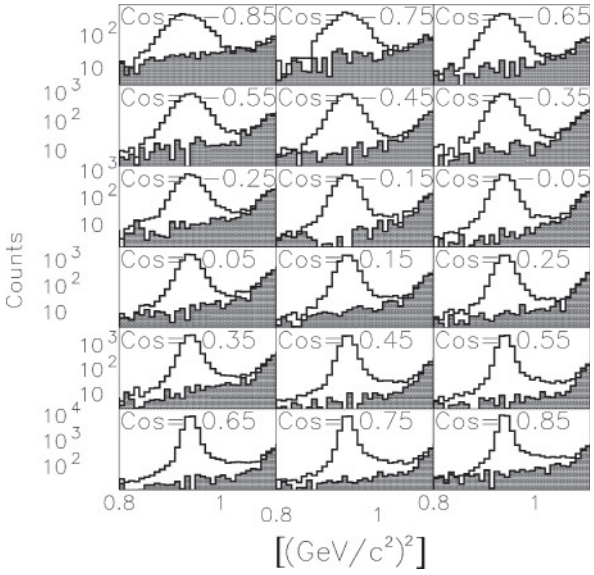

FIG. 3. Neutron yield extraction for $E_\gamma = 1.475$ GeV. The background is represented as the shaded region.

missing mass spectrum in the full spectrometer acceptance for all photon energies is shown in Fig. 2. The neutron peak is clearly seen.

Taking each π^+ event that did not have a matching incident photon as just noted, and integrating over all of the out-of-time (not within the trigger coincidence window) incident photons for that event, determined the distribution of accidental coincidences between CLAS and the photon tagger. In this procedure it is assumed that coupling the out-of-time tagger hits to unmatched pions created a fair representation of the accidental coincidences between CLAS and tagger.

C. Distribution of events into kinematic bins

The events from both the 2.445- and 3.115-GeV data sets, constituting the full missing mass spectrum described in the previous section, were sorted into bins in incident photon energy E_γ and $\cos\theta^\pi_{\text{c.m.}}$. The widths of these "kinematic bins" ($\Delta E_\gamma = 50$ MeV in photon energy and $\Delta \cos\theta^\pi_{\text{c.m.}} = 0.1$) were chosen such that, in general, there were at least 1000 $\pi^+ n$ events in each kinematic bin.

D. Neutron yield

For each kinematic bin, the neutron yield was extracted by removing the background under the peak. We have proceeded with the assumption that the background in the missing mass spectra arises from two particular types of events:

(i) events arising from accidental coincidences between CLAS and the photon tagger, as discussed in the preceding section, and
(ii) events arising from two-pion photoproduction via the reaction $\gamma p \to \pi^+ X$, where $X = p\pi^-$ or $X = n\pi^0$.

The spectrum for accidental coincidences is determined by looking at events that fell outside the designated trigger window. To determine the two-pion background, data for the reaction $\gamma p \to p\pi^-\pi^+$ were selected by requiring that each particle in the final state had to be identified through normal particle identification procedures, that the same incident photon was chosen for each particle, and that the missing mass was consistent with zero. These selected data were used to determine the *shape* of the $X = p\pi^-$ and $X = n\pi^0$ components of the background from two-pion photoproduction. [Owing to $\Delta(1232)$ dominance, the contribution from the $X = n\pi^0$ reaction was assumed to have the same shape as the $X = p\pi^-$ contribution.] This shape was used to generate the background beneath the neutron peak, which was then subtracted from the neutron yield for each kinematic bin. The fractional uncertainty in the background beneath the peak was statistically added in quadrature to the uncertainty in the yield for each kinematic bin. In most cases (>93%), the peak-to-background ratio was greater than 5 to 1; in all cases, the signal-to-background ratio was greater than 1.4 to 1. Figure 3 shows an example of this background removal procedure for all kinematic bins with photon energy $E_\gamma = 1.475$ GeV.

E. Acceptance and efficiency

The spectrometer acceptance for charged pions was determined from the results of Monte Carlo simulations of the CLAS detector response to positive pions. As a preliminary test of the quality of the Monte Carlo representation of the CLAS response to π^+, simulated acceptances for π^+ were compared to empirical measurements based on the reaction $\gamma p \to p\pi^-\pi^+$ for most of the kinematic bins in this study. (Note that the empirical acceptance method is not useful for some regions of phase space owing to limited statistics for those kinematic bins.) Such an empirical check is practical for much of the phase space covered in this experiment because of the large number of events for that final state and because all of the final products leave charged tracks in CLAS, making them easily observable. For the empirical comparison, in addition to the π^+, the proton and π^- were required to be detected in the event and both were assigned the same

photon. The same fiducial cuts applied to the π^+ noted earlier were applied to both reconstructed and CLAS-identified π^+. A missing mass reconstruction from the kinematic information of the proton and π^- was performed to determine whether a π^+ should have been seen in CLAS. The background beneath this peak was removed by subtracting a polynomial fit (of order 3) to the background region from the spectrum.

A comparison of Monte Carlo–simulated events to actual data for the $\gamma p \to p\pi^-\pi^+$ reaction (rebinned as if the π^+ came from the $\gamma p \to n\pi^+$ reaction channel) was performed. Simulated events were obtained by generating 10^7 $\gamma p \to p\pi^-\pi^+$ events that were isotropic in phase space and then processed through a GEANT simulation of CLAS created by the Jefferson Laboratory GSIM working group. In addition to simulating the detector response, the GEANT simulation also included the effects of pion decay. In those kinematic bins where the acceptance was less than 10%, agreement between the empirical and Monte Carlo–simulated acceptances was poor. Thus, an acceptance cut was applied such that only kinematic bins that had acceptances greater than 10%, and had no neighboring bins with acceptances less than 10%, were kept. In addition to this "10% criterion," the bins at $\cos\theta^{\pi}_{\text{c.m.}} > 0.9$ and $\cos\theta^{\pi}_{\text{c.m.}} < -0.9$ were removed, since some portion of these bins would have had acceptances of zero owing to the geometry of CLAS. The fraction of all kinematic bins rejected by the "10% criterion" was 0.195.

The empirically measured and Monte Carlo–simulated acceptances agreed well when these conditions were applied. To quantify this agreement, an "acceptance ratio" was determined, defined as the ratio of the empirical acceptance to the Monte Carlo–simulated acceptance for each photon energy and $\cos\theta^{\pi}_{\text{c.m.}}$ bin (with the acceptance cut applied). These acceptance ratios were placed in a histogram and then fit with a Gaussian. The center of the Gaussian was 0.9997 and the standard deviation was 0.040, which affirms the validity of the Monte Carlo simulation of the response of CLAS to π^+.

In addition to examining the ratio of the empirical acceptance to the Monte Carlo acceptance, a standardized Gaussian distribution z_{ij} was created by forming, for each kinematic bin, the difference of the Monte Carlo–simulated acceptance ϵ_{MC} and the empirical acceptance ϵ_E, with that difference divided by the combined acceptance uncertainty,

$$z_{ij} = \frac{(\epsilon_{ij})_{\text{MC}} - (\epsilon_{ij})_E}{(\sigma_{ij})_{\text{MC+E}}}, \tag{1}$$

where

$$(\sigma_{ij})_{\text{MC+E}} = \sqrt{(\sigma_{ij})^2_{\text{MC}} + (\sigma_{ij})^2_E}, \tag{2}$$

histogrammed for each energy i and $\cos\theta^{p}_{\text{c.m.}}$ j kinematic bin. These points are assumed to obey Gaussian statistics with a variance of one and a centroid located at exactly zero. If the centroid of the distribution has been "pulled" away from zero, that suggests the Monte Carlo acceptance results $(\epsilon_{ij})_{\text{MC}}$ do not approximate the empirical acceptance exactly. If the variance of the z_{ij} distribution is less than one, then the uncertainties $(\sigma_{ij})_{\text{MC+E}}$ are too large. Conversely, if the variance of the z_{ij} distribution is greater than one, this suggests the uncertainties $(\sigma_{ij})_{\text{MC+E}}$ are underestimated.

The uncertainties of the Monte Carlo acceptance are assumed to be well represented by the uncertainty appropriate for a binomial distribution:

$$(\sigma_{ij})_{\text{MC}} = \sqrt{\frac{(\epsilon_{ij})_{\text{MC}}[1 - (\epsilon_{ij})_{\text{MC}}]}{(N_{ij})_{\text{Thrown}}}}, \tag{3}$$

where $(N_{ij})_{\text{Thrown}}$ is the number of events thrown in the ij kinematic bin.

The mean of the standardized Gaussian distribution z_{ij} from Eq. (1) was nearly equal to zero within uncertainties (0.10 ± 0.09). The value of χ^2_{reduced} for the Gaussian fit to the distribution, $\chi^2_{\text{reduced}} = 0.86$, was also reasonable. However, the standard deviation, 1.29 ± 0.09, was larger than the optimal value of one, suggesting that the uncertainties $\sigma_{\text{MC+E}}$ were too small. When an additional 2% uncertainty was added in quadrature to the Monte Carlo uncertainty, the centroid, standard deviation, and χ^2_{reduced} were 0.09 ± 0.07, 1.02 ± 0.05, and 0.514, respectively.

To test how far the Monte Carlo results were from optimal, we added 0.1% to the Monte Carlo efficiency. With this 0.1% shift to the Monte Carlo the centroid, standard deviation, and χ^2_{reduced} were 0.05 ± 0.06, 1.02 ± 0.05, and 0.465, respectively. Since the values are consistent with the optimal values, we assume henceforth that the Monte Carlo acceptances agree very well with the empirical acceptances when 2% additional uncertainty is added to the Monte Carlo acceptances. In the remainder of this analysis it is assumed that it is appropriate to add this extra 2.0% uncertainty in quadrature to the Monte Carlo uncertainties on a bin-by-bin basis and that has been done for each kinematic bin.

Having confirmed the validity of the Monte Carlo representation of the CLAS response to π^+, we obtained the acceptance results for the reaction $\gamma p \to n\pi^+$ by generating 10^7 events (weighted by the cross sections given by the SAID solution [5]) that were then processed in the same manner as the $\gamma p \to p\pi^-\pi^+$ comparison reaction. These simulated acceptances were used to determine the differential cross sections reported here.

F. Sector-by-sector comparison

A sector-by-sector comparison of the differential cross sections was performed to check the consistency of the extracted cross sections. CLAS is constructed from six sectors, which, ideally, should be identical. However, operationally, the response of each sector is different owing to various hardware circumstances, problems, and differences. The simulations described in the previous section incorporate knowledge of the various differences in the sectors to properly reproduce the CLAS response for each particle type. Since the Monte Carlo simulations should reflect sector-by-sector changes in the detector arising from, for example, holes in the drift chamber system from broken wires and bad time-of-flight paddles, a sector-by-sector comparison of the differential cross sections inferred from the data obtained explores the reliability of the Monte Carlo simulation with respect to these detector irregularities. The results of this comparison indicated that variations attributable to sector-by-sector variations were less

than 0.4% and were much smaller than the uncertainty in the cross sections, thus confirming the validity of the simulated sector-by-sector response.

A standardized Gaussian distribution for the sector-by-sector comparison was created by forming, for each photon energy, $\cos\theta^{\pi}_{\text{c.m.}}$, and sector bin, the difference of the differential cross section in each sector to the sector average and dividing the result by the uncertainty.

The resulting centroid, standard deviation, and χ^2_{reduced} of the standardized Gaussian distribution were 0.047 ± 0.021, 0.979 ± 0.018, and 1.01, respectively. Thus, although the χ^2_{reduced} and standard deviation of the Gaussian are reasonable, the centroid is somewhat smaller than the optimal value of zero.

To roughly estimate how far off the cross sections might be from the desired value for the centroid, we shifted the sector average by a factor of 0.996. The resulting modified centroid, standard deviation, and χ^2_{reduced}, were found to be 0.003 ± 0.021, 0.985 ± 0.018, and 0.979, respectively. Since this small shift of 0.4% in the sector average (a shift much smaller than the uncertainty for the cross section) produces parameters for the standardized Gaussian that are within optimal values, the nonshifted parameters are acceptably close to optimal.

G. Bin migration

To estimate the systematic uncertainty associated with bin migration, the acceptance and efficiency results calculated using SAID-weighted events were compared to acceptance and efficiency results using nonweighted events. Since the amount of the correction was found to be typically less than 2%, the systematic uncertainty associated with bin migration was assumed to be ignorable.

H. Trigger inefficiency

The determination of a charged particle trigger inefficiency for the `g1c` data was performed by looking at data from a running period just preceding the `g1c` period, the `g2a` running period. (The `g2a` running period is more fully described in Ref. [21].) This running period had, in addition to the charged particle trigger, a photon trigger. The photon trigger required that there was a hit in any two sectors of the electrocalorimeters located downstream of CLAS in coincidence with a hit in the photon tagger. By looking at `g2a` events that had a photon trigger and no charged trigger, yet had a π^+ in the event, the inefficiency of the charged particle trigger in CLAS for π^+ was determined. This correction was applied to each kinematic bin and was always less than 1.0%.

I. Normalization

The *absolute photon flux* for the entire tagger photon energy range was determined by measuring the rate of scattered electrons detected in each counter of the focal plane of the bremsstrahlung photon tagger by sampling focal plane hits not in coincidence with CLAS. The detection rate for the post-bremsstrahlung scattered electrons was integrated over the lifetime of the experiment and converted to the corresponding total number of photons on target for each counter of the tagger focal plane. The tagging efficiency was measured in dedicated runs with a total absorption counter (TAC) downstream of the cryogenic target, which directly counted all photons in the beam. The details of the method can be found in Ref. [22].

IV. UNCERTAINTIES

We summarize here the various uncertainties present in the cross sections obtained in this work.

(i) An overall estimated systematic uncertainty of 1% is taken as a very conservative estimate of all sources of *trigger inefficiency*, as described in Sec. III H.

(ii) The uncertainties associated with the *detector response, bin migration* and *track reconstruction* are contained within the uncertainties associated with the Monte Carlo acceptance estimates described in Sec. III E. These uncertainties are taken into account on a bin-by-bin basis.

(iii) The uncertainties associated with the *background subtraction* described in Sec. III D are purely statistical, and these were taken into account on a bin-by-bin basis.

(iv) The largest source of uncertainty in the *photon flux normalization* arises from the uncertainty in the measurement of the "tagger efficiency" [7], essentially a measure of the photon beam collimation taken during normalization runs. The value of this tagger efficiency is dependent upon the positioning of the electron beam supplied by the accelerator on the radiator of the photon tagger and will vary on a run-by-run basis determined by the run-by-run condition of the electron beam tune. With the procedure used to obtain the photon flux normalization [22], the statistical uncertainties associated with the photon flux normalization are always far below 1% and, when considered with other uncertainties in the absolute normalization, are negligible.

(v) The systematic uncertainty of the *absolute normalization* comprises six parts; three of them do not vary over the running period, while the remaining three do. The following quantities vary over the running period:
   (a) run-to-run variations in the normalized neutron yield unaccounted for by statistical uncertainties alone,
   (b) uncertainty in the target density [23], and
   (c) statistical uncertainty of the photon flux normalization.

Table I shows contributions to the systematic uncertainties for quantities that varied over the running period.

The following systematic uncertainties do not change over the running period:

(i) uncertainty in the liquid-hydrogen target-cell length, which was 0.3% [24];

(ii) uncertainty associated with the tagger energy calibration (described in Sec. III I), which was less than 1%; and

(iii) uncertainty in the trigger inefficiency correction, which was less than 1%.

After adding all of the systematic uncertainties in quadrature, the systematic uncertainty for the absolute normalization is 1%, 2%, and 4% for the 2.445 GeV, 3.115 GeV (full),

TABLE I. Systematic uncertainties in the absolute normalization for quantities that varied over the running period. (The data set descriptions are discussed in Sec. II.)

Data set	Run-to-run	Target density
2.445	0.9%	0.1%
3.115-full	1.9%	0.3%
3.115-half	3.6%	0.3%

and 3.115 GeV (half) data sets, respectively. However, since combinations of more than one of these data sets was used to obtain the differential cross section for each kinematic bin, a 4% absolute normalization uncertainty is assumed for simplicity.

V. RESULTS

The 618 differential cross sections obtained in this experiment are compared to the world data set [25–45] in Figs. 4–6, along with a number of representative fits described in the following. The differential cross sections reported here are the first tagged $\pi^+ n$ measurements above 780 MeV [45]. The cross sections are available in electronic form in Ref. [47]. The database entries include the differential cross sections, as well as uncertainties (excluding the overall absolute normalization uncertainty), for each incident photon energy and $\cos\theta^{\pi}_{\text{c.m.}}$ bin shown in this paper.

For a specific example of agreement with previous measurements, in Fig. 4 we compare differential cross sections obtained here with those from the A2 Collaboration of the MAMI-B group [45], at an energy common to both experiments. The CLAS data and the results from MAMI-B appear to agree well at this energy.

More generally, as can be seen in Figs. 4–6, agreement with previous measurements is good overall. The largest deviations

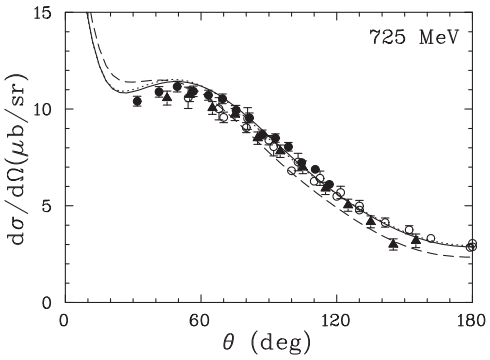

FIG. 4. The differential cross section for $\gamma p \to \pi^+ n$ at $E_\gamma =$ 725 MeV vs pion center-of-mass scattering angle. Solid (dotted) lines correspond to the SAID SP09 (FA07) solution. Dashed lines give the MAID07 [46] predictions. Experimental data are from the current (filled circles) and recent MAMI-B measurements (triangles) at 723 MeV [45]. Previous bremsstrahlung measurements (open circles) are from Refs. [30,32,33,38,43]. The data have been selected from energy bins spanning at most 3 MeV. Plotted uncertainties are statistical.

generally occur at forward angles. Thus further measurements at more forward angles would be useful. Although agreement with previous measurements is generally good, even so, the data here extend measurements to higher energies with more complete angular coverage than obtained in those previous measurements.

VI. AMPLITUDE ANALYSIS OF DATA

We have included the new cross sections from this experiment in a number of multipole analyses covering incident photon energies up to 2.7 GeV using the full SAID database to gauge the influence of the present measurements, as well as their compatibility with previous measurements. A "forced" fit, which included the present data set weighted by an arbitrary factor of 4, was compared to a standard fit. (The standard fit with normal weighting is henceforth called SP09.) The results with two different weightings were in good agreement, despite the CLAS data having a larger weighting. This agreement is not surprising given the agreement of these new data with previously published measurements and that an older fit (FA07) was able to give a reasonable prediction for the previously published cross sections at all but the highest energies [48].

In Table II, we compare SP09 with two previous SAID fits (FA07 and FA06 [5]) and also with the Mainz fit MAID07 [46] up to its stated center-of-mass energy W limit of 2 GeV ($E_\gamma = 1.65$ GeV). The FA07 fit included LEPS Collaboration $\pi^0 p$ measurements [49]. These three solutions are compared with the data in Figs. 5 and 6. Whereas the FA07 and SP09 SAID fits agree well over the energy range of the Mainz fit, disagreements between the SAID and MAID fits are most pronounced at angles more forward than the CLAS data. Near its upper energy limit, the MAID07 solution also exhibits structure not seen in the data.

Above 2.4 GeV, the new CLAS data reported here begin to depart from the FA07 predictions. As a result, the new data presented here have resulted in adjustments of a number of parameters in the SP09 solution so that the new solution better reproduces the measured cross sections, which are significantly lower than the predictions given by FA07.

In fitting the data, the stated experimental systematic uncertainties have been used as an overall normalization adjustment factor for the angular distributions [50]. FA07 included all previously published data used in FA06 [5], plus

TABLE II. χ^2 comparison of fits to pion photoproduction data up to 2.7 GeV. Results are shown for three different SAID (SP09, FA07, and FA06) and recent MAID07 solutions. See text for details. Comparison includes all previous plus new CLAS $\pi^+ n$ measurements.

Solution	Energy limit (MeV)	χ^2/data	Data
SP09	2700	2.11	25639
FA07	2700	2.02	24376
FA06	3000	2.15	25252
MAID07	1650	7.38	22621

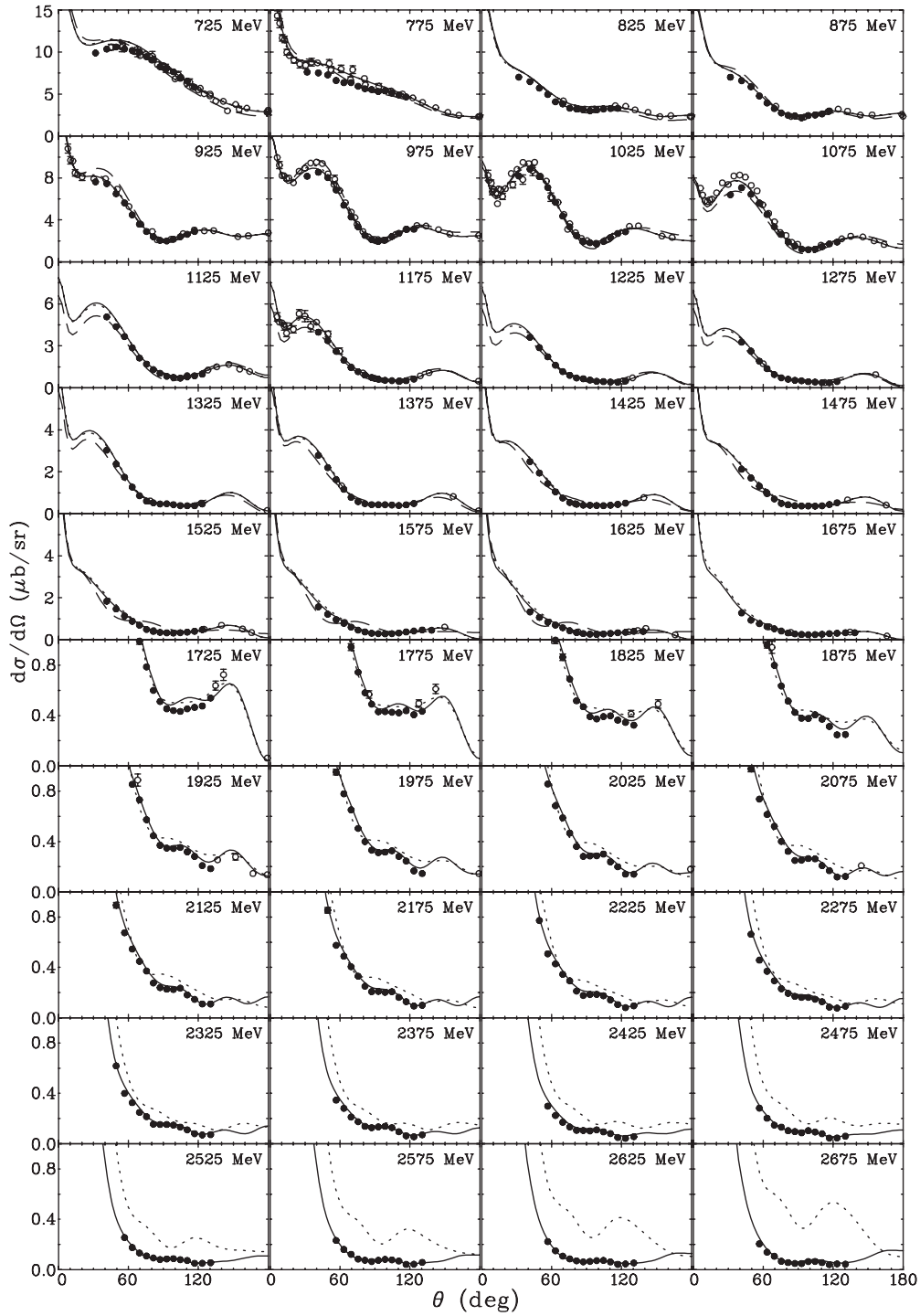

FIG. 5. The differential cross section for $\gamma p \to \pi^+ n$ below $E_\gamma = 2.7$ GeV vs pion center-of-mass scattering angle. Solid (dotted) lines correspond to the SAID SP09 (FA07) solution. Dashed lines give the MAID07 [46] predictions. Experimental data are from the current (filled circles) and previous measurements (open circles). The plotted points from previously published experimental data are those data points within 3 MeV of the photon energy indicated on each panel. Plotted uncertainties are statistical.

recent $\pi^0 p$ differential cross sections and beam asymmetry Σ data from the LEPS Collaboration [49]. The MAID07 analysis does not include the recent $\pi^0 p$ measurements from CLAS [5] and LEPS [49] and has a center-of-mass energy limit of $W = 2$ GeV ($E_\gamma = 1.65$ GeV). Presently, the pion photoproduction database below $E_\gamma = 2.7$ GeV consists of 25,639 data points that have been fit in the SP09 solution with $\chi^2 = 54161$. The contribution to the total χ^2 in the SP09 analysis of the 561 new CLAS $\pi^+ n$ data points (e.g., those data points up to $E_\gamma = 2.7$ GeV) is 1407.

Multipoles from the SP09 fit are compared to the earlier MAID07 determinations in Figs. 7 and 8. Both FA07 and

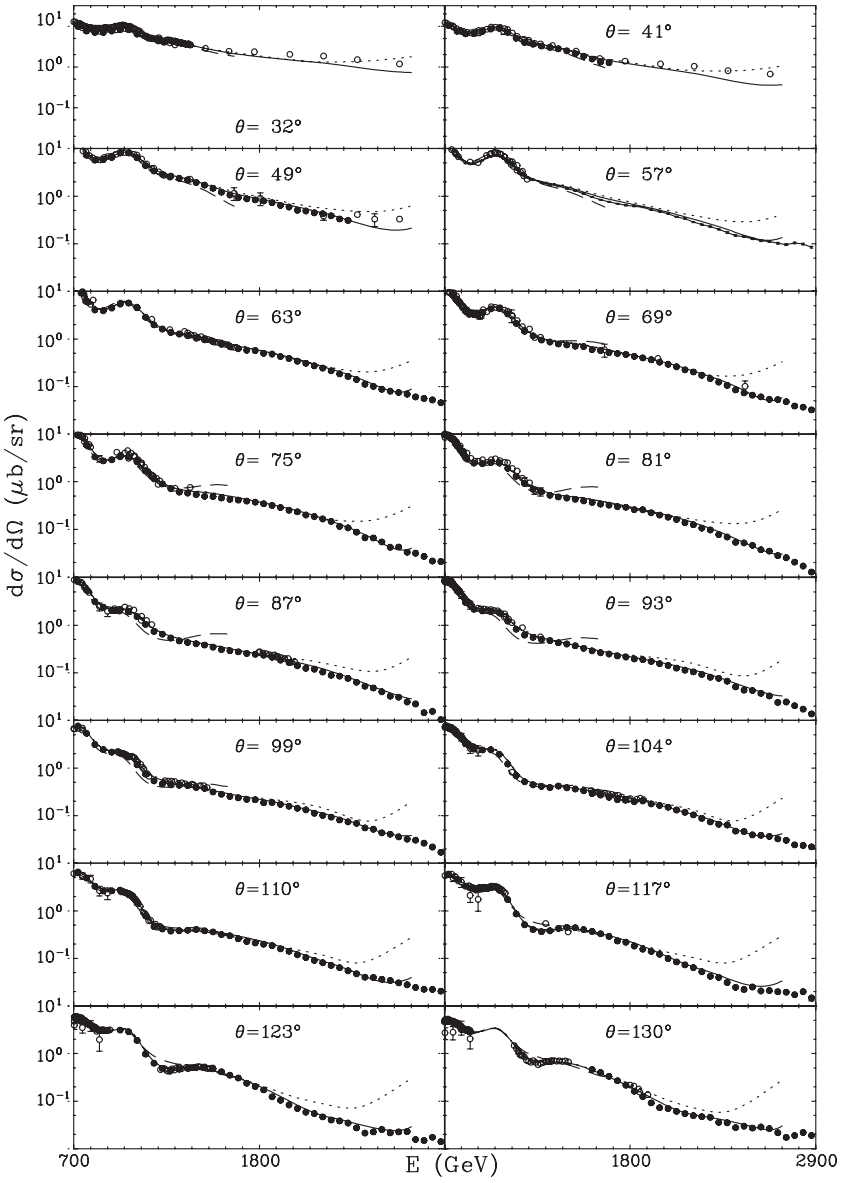

FIG. 6. Fixed angle excitation functions for $\gamma p \to \pi^+ n$. The pion center-of-mass scattering angle is shown. Notation is as in Fig. 5. The plotted points from previously published experimental data are those data points within 2° of the angle indicated on each panel.

SP09 are quite similar, but significant differences between SAID and MAID in magnitude (e.g., $E_{2-}^{1/2}$, $M_{2-}^{3/2}$, and $E_{3-}^{3/2}$) and W dependance (e.g., $M_{1+}^{1/2}$ and $M_{1-}^{3/2}$) are seen. Given that large differences are not seen in the differential cross sections, further measurements of spin observables will be needed to better constrain these amplitudes.

With the addition of CLAS $\pi^0 p$ and $\pi^+ n$ cross sections, the SAID solution at higher energies is now far more reliable than in previously published analyses. Based on the earlier SAID SM05 solution, the authors of Ref. [52] previously noted how well the single-pion component of the Gerasimov-Drell-Hearn (GDH) sum rule integrand reproduced the full result (including multipion and other-meson production). In Fig. 9, we extend this same comparison significantly beyond the 2 GeV range of the SM05 solution. As seen in the figure, the SP09 solution now agrees well with the MAID07 result, but it extends that result to much higher E_γ. General agreement with the existing GDH data [53] is good.

For completeness, we provide in Fig. 10 a comparison between the predictions for the beam asymmetry Σ from the FA07, MAID07, and SP09 analyses and the experimental data for that variable from GRAAL [54], from DNPL [55], and from CEA [56] for the $\gamma + p \to \pi^+ n$ reaction under study here. The agreement with the GRAAL data for Σ at 1.3 GeV is very good for both SAID solutions, but there are discrepancies at center-of-mass scattering angles greater than 75° between those data and the MAID07 predictions. All three analyses are seen to match the single Σ data point from CEA at 1.6 GeV, and both the FA07 and SP09 analyses provide reasonably good predictions for the DNPL data for Σ for positive pions at 2.1 GeV [55], although the agreement is poorer for center-of-mass scattering angles greater than 75°. However, the data for Σ remain relatively sparse compared to the existing data for the differential cross sections. New data for Σ will help firm up the experimental situation for this energy region, and a number of experiments are underway at Jefferson Lab to obtain such data for pions and other mesons [57,58].

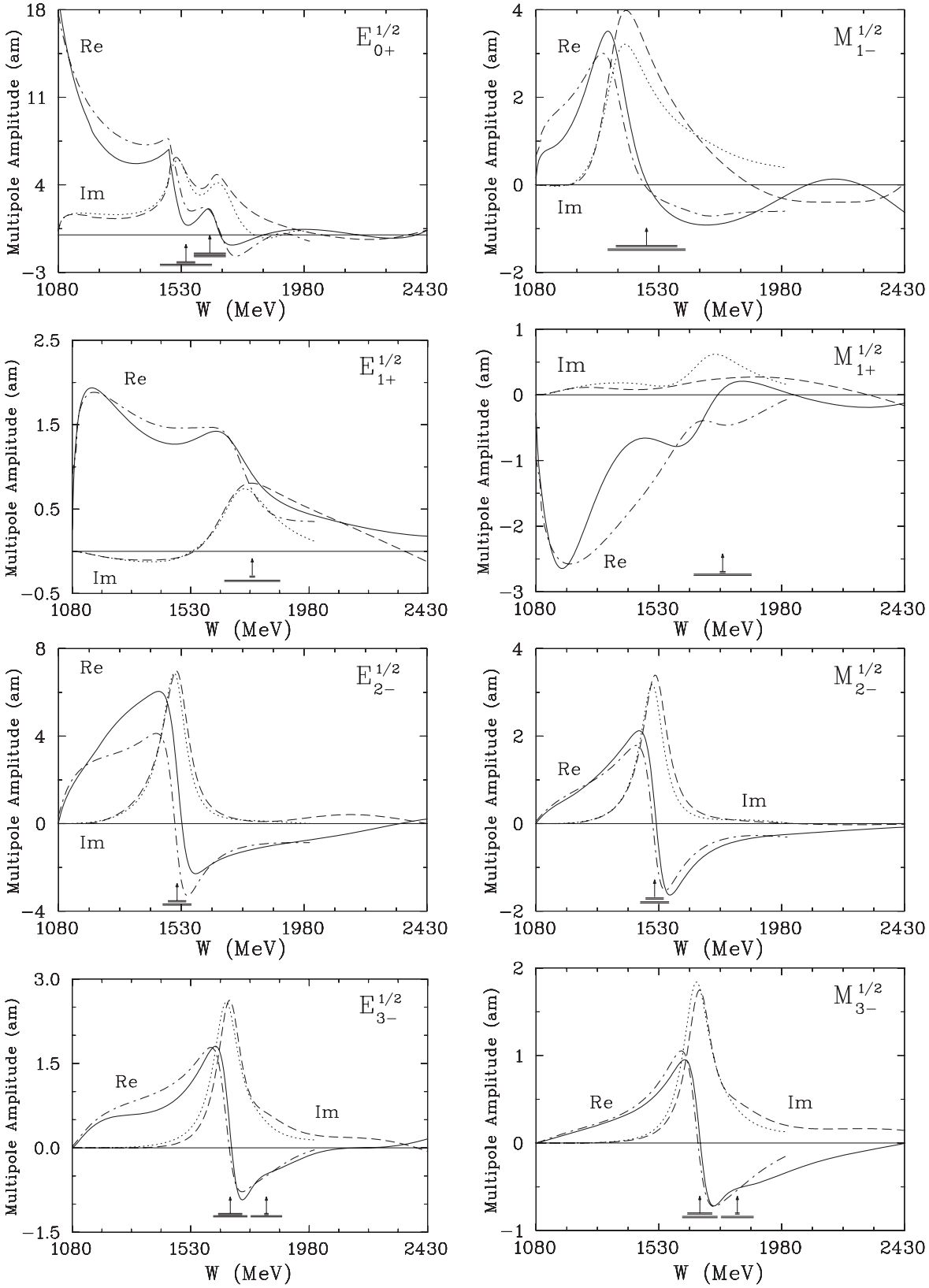

FIG. 7. Multipole amplitudes from threshold to $E_\gamma = 2.7$ GeV for isospin 1/2. Solid (dashed) lines correspond to the real (imaginary) part of the SP09 solution. Dashed-dot (dotted) lines give real (imaginary) part of the MAID07 [46] solution. Vertical arrows indicate W_R and horizontal bars show full Γ and partial widths for $\Gamma_{\pi N}$ associated with the SAID πN solution SP06 [51].

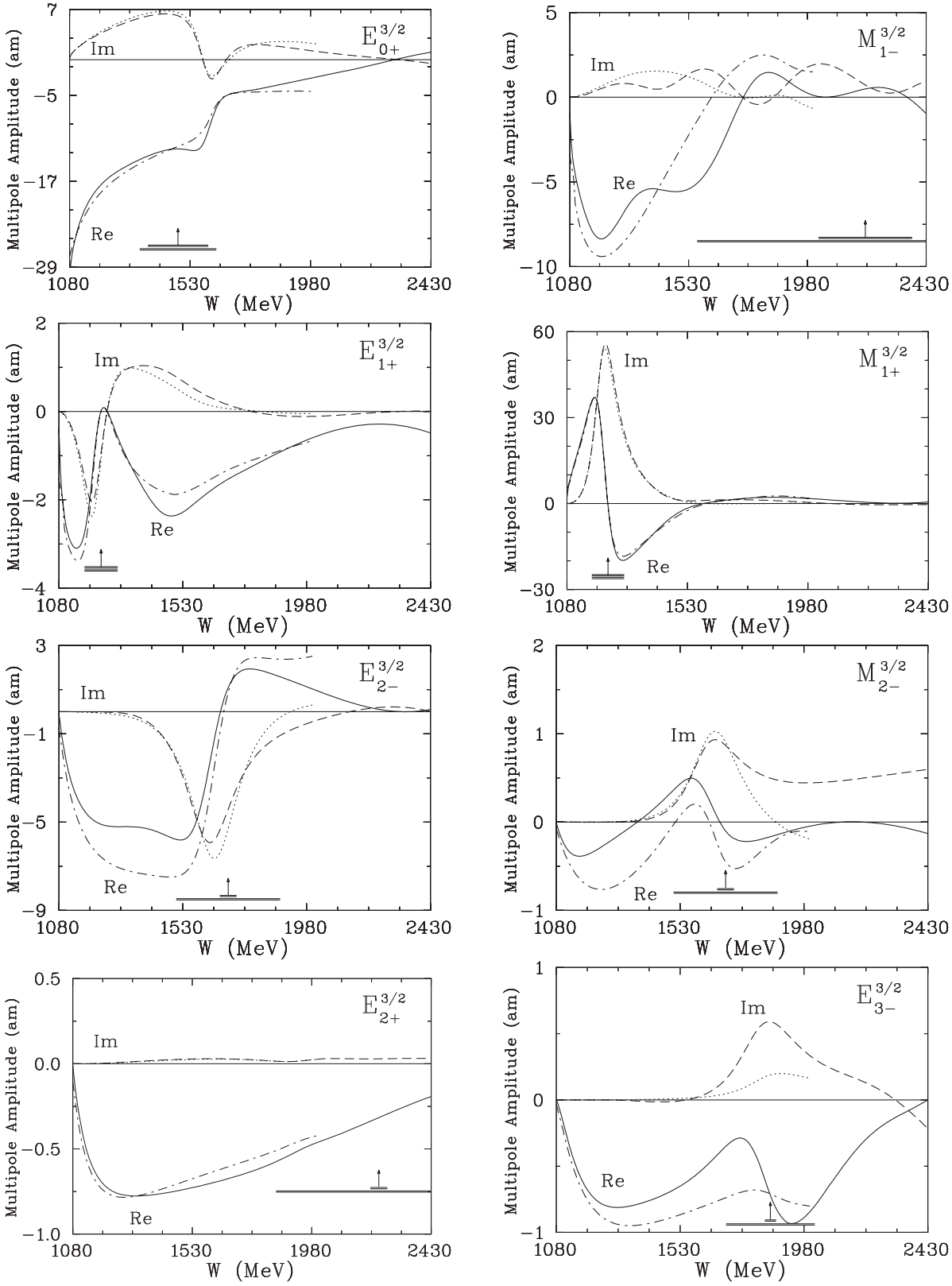

FIG. 8. Multipole amplitudes from threshold to $E_\gamma = 2.7$ GeV for isospin 3/2. Notation is as in Fig. 7.

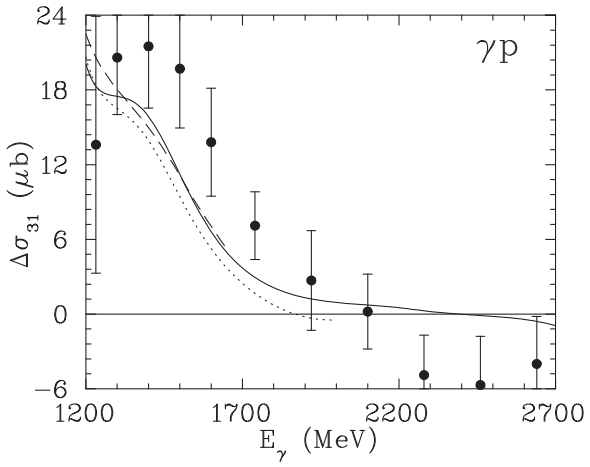

FIG. 9. Single-pion photoproduction contributions to the proton GDH sum rule $\Delta\sigma_{31} = \sigma_{3/2} - \sigma_{1/2}$ from the SAID current (solid), recently published SM05 [52] (dotted), and MAID07 [46] (dashed) analyses. GDH data are from Ref. [53]. Plotted uncertainties are statistical and systematical added in quadrature.

VII. RESONANCE COUPLINGS

As in Ref. [5], we have extracted resonance couplings from the modified fit (SP09) using a simple resonance plus background assumption, a form similar to that used in the MAID analysis,

$$B(W)(1 + iT_{\pi N}) + T_{\rm BW}e^{i\phi}, \tag{4}$$

where $T_{\pi N}$ is the associated full pion-nucleon T-matrix and $T_{\rm BW}$ is a Breit-Wigner parametrization of the resonance contribution. With this model, resonance contributions have been determined and are listed in Table III. Values for the resonance mass W_R, width Γ, and branching fraction $\Gamma_{\pi N}/\Gamma$ for the various resonances were taken from a recent SAID analysis of pion-nucleon elastic scattering data [51]. These couplings were also calculated in Ref. [5] after the addition of $\pi^0 p$ photoproduction data reported in that reference.

The function $B(W)$ was fit to data over an energy range spanning the resonance position. In the MAID determination, $B(W)$ was given by the Born term. Differences between the couplings quoted here and in MAID therefore reflect both the impact of the present data set and a model-dependent uncertainty associated with the resonance extraction procedure.

Results based on a fit not including the present data set, presented in Ref. [5], generally fall within one to three standard deviations of the present values. This stability is to be expected; larger deviations may occur with the addition of forthcoming polarization measurements.

However, the range of couplings given in Table III requires further comment. The two resonances coupled to a $\pi N S_{11}$ state are given very different estimates in the present analysis than those provided by the 2007 MAID fit and the Particle Data Group (PDG). The PDG range for the $N(1535)$ accounts for the large discrepancy that once existed between determinations based on πN and ηN photoproduction fits. Whereas the present πN estimate, the PDG central value, and older ηN photoproduction analyses agree on a value close to

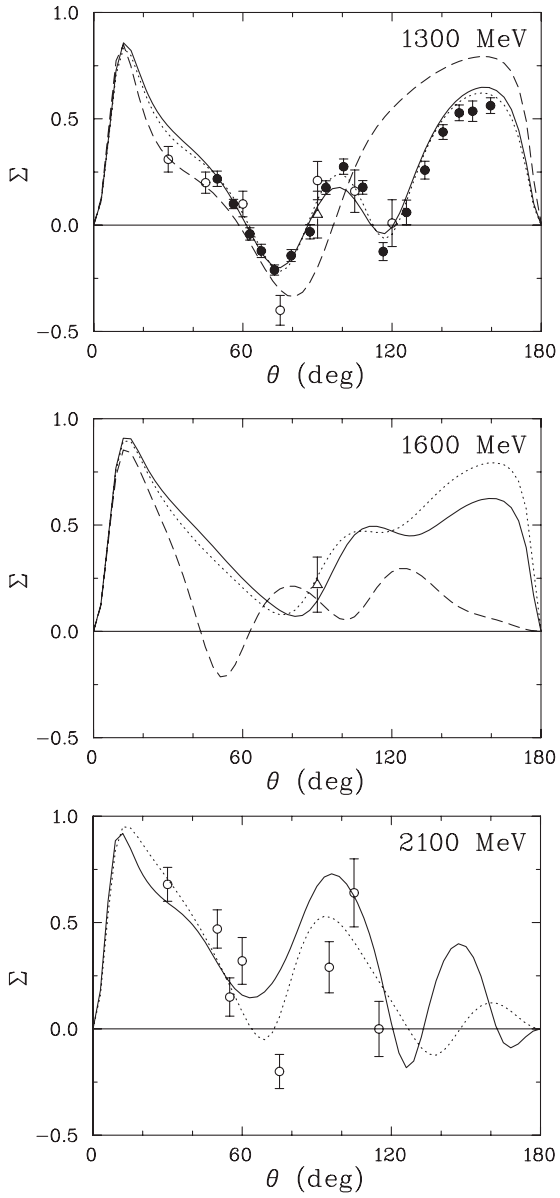

FIG. 10. Beam asymmetry Σ for $\gamma p \to \pi^+ n$ at $E_\gamma =$ 1300, 1600, and 2100 MeV vs center-of-mass scattering angle. Solid (dotted) lines correspond to the SAID SP09 (FA07) solution. Dashed lines give the MAID07 [46] predictions. Experimental data are from GRAAL (filled circles) [54], from DNPL (open circles) [55], and from CEA (open triangles) [56]. Plotted uncertainties are statistical. Systematic uncertainties are taken into account in the fit (see text).

100 GeV$^{-1.2} \times 10^{-3}$, the MAID 2007 value has now dropped to a value consistent with the 1996 SAID value [59]. This low value was criticized in a number of papers analyzing ηN photoproduction data measured at MAMI-B in Mainz [60].

From the plots in Figs. 7 and 8, a significant difference between the SAID and MAID fits exists in multipoles coupled to the $\pi N S_{11}$ and D_{13} resonances. This, combined with differences in the assumed background contribution, likely accounts for the variations seen in Table III. Differences in the $N(1650)$ couplings are largely due to difficulties in separating two nearby resonances in a single multipole. The present

TABLE III. Resonance parameters for N^* and Δ^* from the SAID fit to the πN data [51], helicity amplitudes $A_{1/2}$ and $A_{3/2}$ from the SP09 solution, MAID07 determination [46], and average values from Ref. [4].

Resonance	πN SAID			$A_{1/2}$ (GeV$^{-1/2} \times 10^{-3}$)			$A_{3/2}$ (GeV$^{-1/2} \times 10^{-3}$)		
	W_R (MeV)	Γ (MeV)	Γ_π/Γ	SP09	MAID07	PDG	SP09	MAID07	PDG
$N(1535)S_{11}$	1547	188	0.36	100.9 ± 3.0	66	90 ± 30			
$N(1650)S_{11}$	1635	115	1.00	9.0 ± 9.1	33	53 ± 16			
$N(1440)P_{11}$	1485	284	0.79	-56.4 ± 1.7	-61	-65 ± 4			
$N(1720)P_{13}$	1764	210	0.09	90.5 ± 3.3	73	18 ± 30	-36.0 ± 3.9	-11	-19 ± 20
$N(1520)D_{13}$	1515	104	0.63	-26 ± 1.5	-27	-24 ± 9	141.2 ± 1.7	161	166 ± 5
$N(1675)D_{15}$	1674	147	0.39	14.9 ± 2.1	15	19 ± 8	18.4 ± 2.1	22	15 ± 9
$N(1680)F_{15}$	1680	128	0.70	-17.6 ± 1.5	-25	-15 ± 6	134.2 ± 1.6	134	133 ± 12
$\Delta(1620)S_{31}$	1615	147	0.32	47.2 ± 2.3	66	27 ± 11			
$\Delta(1232)P_{33}$	1233	119	1.00	-139.6 ± 1.8	-140	-135 ± 6	-258.9 ± 2.3	-265	-250 ± 8
$\Delta(1700)D_{33}$	1695	376	0.16	118.3 ± 3.3	226	104 ± 15	110.0 ± 3.5	210	85 ± 22
$\Delta(1905)F_{35}$	1858	321	0.12	11.4 ± 8.0	18	26 ± 11	-51.0 ± 8.0	-28	-45 ± 20
$\Delta(1950)F_{37}$	1921	271	0.47	-71.5 ± 1.8	-94	-76 ± 12	-94.7 ± 1.8	-121	-97 ± 10

$N(1650)$ photo-decay amplitude is consistent with that found in Ref. [5], given the large errors. The statistical significance of any inconsistencies with the MAID analysis cannot be determined, as no uncertainties for their estimates have been presented.

Both the SAID and MAID values for the $N(1720)$ coupling are very different from the PDG average. The PDG range does not even include a sign for this coupling. As this state has the lowest πN branching fraction listed in Table III, a better determination may require a more favorable reaction or additional information on spin observables. Finally, we note that, although the present SAID fit, the fit in Ref. [5], and the PDG estimate for the $\Delta(1700)$ photo-decay amplitudes have remained relatively stable, the MAID 2007 value for the $A_{1/2}$ amplitude has nearly doubled the MAID 2003 result. This change has resulted in both the helicity 1/2 and 3/2 couplings being more than double the PDG estimate.

VIII. CONCLUSION

Differential cross sections for π^+ meson photoproduction on the proton via the reaction $\gamma p \to n\pi^+$ have been determined with a tagged-photon beam for incident photon energies from 0.725 to 2.875 GeV. All derived cross sections were based on a $\pi^+ n$ missing mass reconstruction. The relative cross sections were determined from yields derived from a peak isolated above a well-determined background, using Monte Carlo simulations to determine the π^+ acceptance in the CLAS spectrometer. The relative differential cross sections were converted to absolute differential cross sections by measurements of the incident photon flux.

These data have been included in a SAID multipole analysis, resulting in a new SAID solution, SP09. Comparisons to earlier SAID fits and a fit from the Mainz group show that the new solution is much more satisfactory at higher energies. Although resonance couplings have not changed significantly with the addition of these cross sections to the world data set, significant changes have occurred in the high-energy behavior of the SAID cross-section predictions and amplitudes, as can be seen in Fig. 5 for the cross-section contribution and Fig. 9 for the single-pion contribution to the GDH sum rule. Further improvement will be possible with future measurements of spin observables for the photoproduction process that can be expected from FROST [57] and the g8b CLAS running period [58].

ACKNOWLEDGMENTS

The authors gratefully acknowledge the work of the Jefferson Lab Accelerator Division staff. This work was supported by the National Science Foundation, the U.S. Department of Energy (DOE), the French Centre National de la Recherche Scientifique and Commissariat à l'Energie Atomique, the Italian Istituto Nazionale di Fisica Nucleare, and the Korean Science and Engineering Foundation. The Southeastern Universities Research Association (SURA) operated Jefferson Lab for DOE under Contract No. DE-AC05-84ER40150 during this work.

[1] T. Mart and A. Sulaksono, Phys. Rev. C **74**, 055203 (2006); B. Julia-Diaz, B. Saghai, T. S. H. Lee, and F. Tabakin, *ibid.* **73**, 055204 (2006); V. Kuznetsov *et al.*, Phys. Lett. **B647**, 23 (2007); A. Fix, L. Tiator, and M. V. Polyakov, Eur. Phys. J. A **32**, 311 (2007); V. Shklyar, H. Lenske, and U. Mosel, Phys. Lett. **B650**, 172 (2007).

[2] S. Capstick and W. Roberts, Prog. Part. Nucl. Phys. **45**, S241 (2000).

[3] R. A. Arndt, W. J. Briscoe, I. I. Strakovsky, and R. L. Workman, Phys. Rev. C **66**, 055213 (2002); D. Drechsel, S. S. Kamalov, and L. Tiator, Eur. Phys. J. A **34**, 69 (2007); G. Penner and U. Mosel, Phys. Rev. C **66**, 055212 (2002); T. P. Vrana, S. A. Dytman, and T. S. H. Lee, Phys. Rep. **328**, 181 (2000).

[4] C. Amsler *et al.* (Particle Data Group), Phys. Lett. **B667**, 1 (2008); http://pdg.lbl.gov/.

[5] M. Dugger *et al.* (CLAS Collaboration), Phys. Rev. C **76**, 025211 (2007).
[6] B. A. Mecking *et al.* (CLAS Collaboration), Nucl. Instrum. Methods A **503**, 513 (2003).
[7] D. I. Sober *et al.*, Nucl. Instrum. Methods A **440**, 263 (2000).
[8] R. Bradford *et al.* (CLAS Collaboration), Phys. Rev. C **73**, 035202 (2006).
[9] M. Dugger *et al.* (CLAS Collaboration), Phys. Rev. Lett. **96**, 062001 (2006).
[10] S. Strauch *et al.* (CLAS Collaboration), Phys. Rev. Lett. **95**, 162003 (2005).
[11] J. W. C. McNabb *et al.* (CLAS Collaboration), Phys. Rev. C **69**, 042201 (2004).
[12] M. Battaglieri *et al.* (CLAS Collaboration), Phys. Rev. Lett. **90**, 022002 (2002).
[13] M. Dugger *et al.* (CLAS Collaboration), Phys. Rev. Lett. **89**, 222002 (2002).
[14] M. Battaglieri *et al.* (CLAS Collaboration), Phys. Rev. Lett. **87**, 172002 (2001).
[15] E. Anciant *et al.* (CLAS Collaboration), Phys. Rev. Lett. **85**, 4682 (2000).
[16] S. Taylor *et al.* (CLAS Collaboration), Nucl. Instrum. Methods A **462**, 484 (2001).
[17] M. D. Mestayer *et al.*, Nucl. Instrum. Methods A **449**, 81 (2000).
[18] E. S. Smith *et al.*, Nucl. Instrum. Methods A **432**, 265 (1999).
[19] E. Pasyuk, CLAS note 2007–008, http://www1.jlab.org/ul/Physics/Hall-B/clas/public/2007-008.pdf.
[20] E. Pasyuk, CLAS note 2007–016, http://www1.jlab.org/ul/Physics/Hall-B/clas/public/2007-016.pdf.
[21] M. Mirazita *et al.* (CLAS Collaboration), Phys. Rev. C **70**, 014005 (2004).
[22] J. Ball and E. Pasyuk, CLAS note 2005–002, http://www.jlab.org/Hall-B/notes/clas_notes05/2005-002.pdf.
[23] R. Bradford and R. A. Schumacher, CLAS note 2002–003, http://www.jlab.org/Hall-B/notes/clas_notes02/02-003.pdf.
[24] R. A. Schumacher, http://www.jlab.org/ccc/mail_archives/CLAS/clas_hadron/msg00325.html.
[25] J. H. Boyden, Ph.D. thesis, California Institute of Technology, 1962 (unpublished).
[26] J. R. Kilner, Ph.D. thesis, California Institute of Technology, 1963 (unpublished).
[27] G. Buschhorn *et al.*, Phys. Rev. Lett. **17**, 1027 (1966).
[28] S. D. Ecklund and R. L. Walker, Phys. Rev. **159**, 1195 (1967).
[29] G. Buschhorn *et al.*, Phys. Rev. Lett. **18**, 571 (1967).
[30] C. Betourne *et al.*, Phys. Rev. **172**, 1343 (1968).
[31] R. A. Alvarez *et al.*, Phys. Rev. D **1**, 1946 (1970).
[32] B. Bouquet, Preprint LAL 1252 (1971).
[33] T. Fujii *et al.*, Phys. Rev. Lett. **26**, 1672 (1971).
[34] K. Ekstrand *et al.*, Phys. Rev. D **6**, 1 (1972).
[35] L. O. Abrahamian *et al.*, Phys. Lett. **B48**, 463 (1974).
[36] I. Arai *et al.*, J. Phys. Soc. Jpn. **43**, 363 (1977).
[37] T. Fujii *et al.*, Nucl. Phys. **B120**, 395 (1977).
[38] E. J. Durwen, Ph.D. thesis, BONN–IR–80–7, Bonn University, 1980.
[39] M. Althoff *et al.*, Z. Phys. C **18**, 199 (1983).
[40] W. Heise, Ph.D. thesis, BONN–IR–88–06, Bonn University, 1988.
[41] P. Zenz, Ph.D. thesis, BONN–IR–88–12, Bonn University, 1988.
[42] K. Buchler *et al.*, Nucl. Phys. **A570**, 580 (1994).
[43] H. W. Dannhausen *et al.*, Eur. Phys. J. A **11**, 441 (2001).
[44] L. Y. Zhu *et al.* (JLab Hall A Collaboration), Phys. Rev. C **71**, 044603 (2005).
[45] J. Ahrens *et al.* (A2 Collaboration), Phys. Rev. C **74**, 045204 (2006).
[46] D. Drechsel, S. S. Kamalov, and L. Tiator, Eur. Phys. J. A **34**, 69 (2007).
[47] The CLAS database archives all data from CLAS: http://clasweb.jlab.org/physicsdb.
[48] The full database and numerous partial-wave analyses can be accessed via secure shell at gwdac.phys.gwu.edu, with userid "said" (no password) or at the SAID Web site: http://gwdac.phys.gwu.edu.
[49] M. Sumihama *et al.* (LEPS Collaboration), Phys. Lett. **B657**, 32 (2007).
[50] R. Arndt, W. Briscoe, I. Strakovsky, and R. Workman, Phys. Rev. C **66**, 055213 (2002).
[51] R. A. Arndt, W. J. Briscoe, I. I. Strakovsky, and R. L. Workman, Phys. Rev. C **74**, 045205 (2006).
[52] R. A. Arndt, W. J. Briscoe, I. I. Strakovsky, and R. L. Workman, Phys. Rev. C **72**, 058203 (2005).
[53] H. Dutz *et al.* (GDH Collaboration), Phys. Rev. Lett. **93**, 032003 (2004).
[54] V. Kuznetsov (GRAAL Collaboration), in *Proceedings of the Workshop on the Physics of Excited Nucleons (NSTAR2001), Mainz, Germany, 2001*, edited by D. Drechsel and L. Tiator (World Scientific, Singapore, 2001), p. 267; V. Kuznetsov (private communication, 2001).
[55] P. J. Bussey *et al.*, Nucl. Phys. **B154**, 205 (1979).
[56] J. Alspector *et al.*, Phys. Rev. Lett. **28**, 1403 (1972).
[57] Experiments with the FROzen Spin Target (FROST) facility in Hall B at Jefferson Lab include the following: F. J. Klein and L. Todor, Jefferson Lab Proposal, E–02–112, Newport News, VA, USA, 2002, http://www.jlab.org/exp_prog/CEBAF_EXP/E02112.html; N. Benmouna, W. J. Briscoe, I. I. Strakovsky, S. Strauch, and G. V. O'Rielly, Jefferson Lab Proposal, E–03–105, Newport News, VA, USA, 2003, http://www.jlab.org/exp_prog/CEBAF_EXP/E03105.html; D. I. Sober, M. Khandaker, and D. G. Crabb, Jefferson Lab Proposal, E–04–102, update to E–91–015 and E–01–104, Newport News, VA, USA, 2004, http://www.jlab.org/exp_prog/CEBAF_EXP/E04102.html; M. Dugger and E. Pasyuk, Jefferson Lab Proposal, E–05–012, Newport News, VA, USA, 2005, http://www.jlab.org/exp_prog/CEBAF_EXP/E05012.html; V. Crede, M. Bellis, and S. Strauch, Jefferson Lab Proposal, E–06–013, Newport News, VA, USA, 2006, http://www.jlab.org/exp_prog/CEBAF_EXP/E06013.html.
[58] P. Collins and M. Dugger, CAA–HS06–03, Jefferson Lab, Newport News, VA, USA, 2006.
[59] R. A. Arndt, I. I. Strakovsky, and R. L. Workman, Phys. Rev. C **53**, 430 (1996).
[60] B. Krusche *et al.*, Phys. Rev. Lett. **74**, 3736 (1995).